

# DEVELOPMENT OF A ROBUST QUASI-POLOIDAL COMPACT STELLARATOR

DENNIS J. STRICKLER,\* STEVEN P. HIRSHMAN, DONALD A. SPONG, MICHAEL J. COLE, JAMES F. LYON, BRADLEY E. NELSON, and DAVID E. WILLIAMSON  
Oak Ridge National Laboratory, Oak Ridge, Tennessee 37831

ANDREW S. WARE *University of Montana, Missoula, Montana 59812*

Received April 14, 2003

Accepted for Publication July 18, 2003

*A compact quasi-poloidally symmetric stellarator (QPS) plasma and coil configuration is described that has desirable physics properties and engineering feasibility with a very low aspect ratio plasma bounded by good magnetic flux surfaces both in vacuum and at  $\langle\beta\rangle = 2\%$ . The plasma is robust with respect to variations of pressure and the resulting bootstrap current, which leave the bounding flux surface approximately unchanged and thus reduce active positional control requirements. This configuration was developed by reconfiguring the QPS modular coils and applying a new computational method that maximizes the volume of good (integrable) vacuum flux surfaces as a measure of robustness. The stellarator plasma and coil design code STELLOPT is used to vary the coil geometry to determine the plasma geometry and profiles that optimize plasma performance with respect to neoclassical transport, infinite- $n$  ballooning stability up to  $\langle\beta\rangle = 2\%$ , and coil engineering parameters. The normal component of the vacuum magnetic field is simultaneously minimized at the full-beta plasma boundary.*

**KEYWORDS:** stellarator design, compact stellarator, stellarator optimization

## I. INTRODUCTION

Compact stellarators are toroidal confinement devices with a low aspect ratio  $A = \langle R \rangle / \langle a \rangle \leq 5$ , a small number of toroidal field periods ( $2 \leq N_p \leq 5$ ), and a bootstrap current producing a small fraction of the magnetic rotational transform. The presence of a small bootstrap current has been necessary to achieve desirable

physics properties at low aspect ratios. Here,  $\langle R \rangle$  and  $\langle a \rangle$  are the average major and minor radii of the noncircular and nonaxisymmetric stellarator plasma. Compact stellarators have been developed to combine the advantages of stellarators (in particular, steady-state operation and the avoidance of disruptions) and tokamaks (e.g., good particle and energy confinement at high beta) in a low-aspect-ratio plasma configuration. Specific examples are the National Compact Stellarator Experiment<sup>1</sup> (NCSX), a three-field-period proof-of-principle device with  $A = 4.4$ , and the Quasi-Poloidal Stellarator<sup>2</sup> (QPS), a two-field-period concept exploration experiment with  $A = 2.7$ .

Numerical optimizations of three-dimensional (3-D) plasmas,<sup>3</sup> and the magnetic coil systems required to support them,<sup>4,5</sup> have led to important advances in the design of high-aspect-ratio stellarators such as Wendelstein 7-X (Ref. 6). Recently, the STELLOPT stellarator optimization code<sup>7</sup> has been used for low-aspect-ratio NCSX and QPS designs to determine the shape of the outer magnetic flux surface, together with internal plasma pressure and current profiles that produce desirable physics properties such as confined particle drift trajectories and plasma stability at  $\langle\beta\rangle \sim 2$  to 4%. The integration of the COILOPT coil model,<sup>8</sup> which includes explicit representations for modular coils as well as coil geometry constraints, into the stellarator optimization package STELLOPT provides a unique and important computational tool for the design of compact stellarators. This self-consistent analysis ensures that physics and engineering criteria are simultaneously targeted in the full-pressure, full-current plasma-coil configuration. The merged analysis uses a parallel version of the Levenberg-Marquardt algorithm,<sup>9</sup> and it is implemented only after separate plasma and coil optimizations have identified an initial configuration with promising physics and engineering properties. The designs for the quasi-axisymmetric NCSX and the quasi-poloidally symmetric QPS were obtained using this merged optimization procedure.

\*E-mail: stricklerdj@ornl.gov

The STELLOPT/COILOPT design approach<sup>10</sup> simultaneously optimizes plasma properties together with coil engineering characteristics. For each evaluation of the physics and engineering targets, the equilibrium magnetic field is provided by the VMEC code,<sup>11</sup> which assumes the existence of nested, island-free magnetic flux surfaces. Following this analysis, two important stellarator design issues remain: (a) the existence of nested, nearly integrable (nonergodic), magnetic flux surfaces and (b) the flexibility and robustness of the coil design with respect to variations in  $\langle\beta\rangle$  and plasma current. Original work<sup>12</sup> to reduce islands in vacuum, and more recent work<sup>13</sup> at nonzero beta, offer a solution to the first of these problems. Island reduction is routinely applied to candidate NCSX coil configurations. In this paper we describe a method that addresses the second issue. It is based on including—in addition to the usual plasma confinement and stability properties at the full value of  $\langle\beta\rangle$ —a vacuum field condition that drives the combined optimization of the plasma and coil configuration into a region of parameter space with improved robustness and flexibility. In Sec. II the optimization of plasma and coils is reviewed, and in Sec. III the vacuum field target is described. Application of the technique to designing a QPS with improved physics and engineering properties is presented in Sec. IV.

## II. INTEGRATED OPTIMIZATION OF PLASMA AND COILS

The compact stellarators and coils developed here were determined by a series of separate optimization steps. First, a fixed-boundary plasma configuration was determined—independent of coils—using STELLOPT. This was followed by a COILOPT optimization to determine a candidate set of coils to approximately reproduce the desired plasma. These coils were subsequently refined by a combined plasma and coil optimization, using the merged STELLOPT/COILOPT code.

The configuration of coils and plasma used in the optimization are shown schematically in Fig. 1. The QPS coil set consists of modular coils to provide the helical field, together with toroidal field (TF) coils and vertical field (VF) coils for configurational flexibility. The coil design is subject to engineering constraints such as minimum coil-coil and coil-plasma separation and minimum coil radius of curvature. The contours in Fig. 1 indicate the values of  $|\mathbf{B}|$  on the outer surfaces of the plasma. The degree of quasi-poloidal symmetry is difficult to infer from Fig. 1. As indicated in Fig. 2, the energy in those Fourier modes of  $|\mathbf{B}|$  that depart from this symmetry rapidly decay away from the boundary toward the magnetic axis.

In the STELLOPT code, the optimization is formulated as a least-squares minimization of a target  $\chi^2 = \sum \chi_i^2(\mathbf{x})$ , where the individual components  $\chi_i$  are gener-

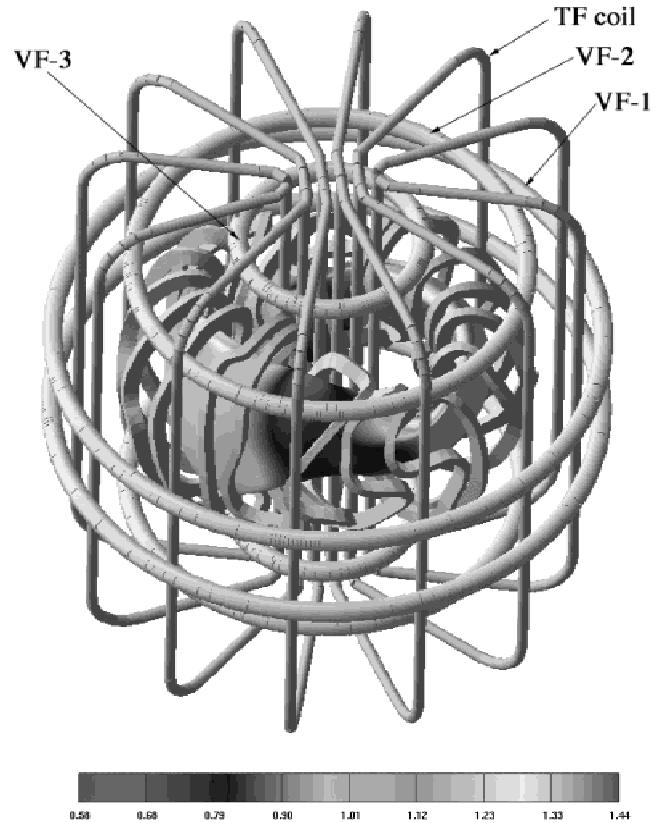


Fig. 1. A compact QPS stellarator plasma and coil configuration. The bar below the figure indicates the range of values of  $|\mathbf{B}|$  (T) on the last closed flux surface. The plasma properties are predominantly determined by the nonplanar (“modular”) coils surrounding the plasma. The circular coils above and below the plasma are the VF coils, and the vertical coils are the TF coils.

ally nonlinear functions of the system state vector  $\mathbf{x}$ . Prior to merging with COILOPT, the state vector  $\mathbf{x}$ , whose components are the independent variables, included coefficients describing the magnetohydrodynamic (MHD) plasma equilibrium pressure and current profiles, as well as either (a) Fourier coefficients of the plasma shape, in the case of a fixed-boundary optimization, or (b) external coil currents, if the optimization was executed in free-boundary mode. The functions  $\chi_i$  include both stellarator physics and coil engineering figures of merit that are evaluated numerically using a set of models dependent on the solution of a three-dimensional (3-D) plasma MHD equilibrium. For example, neoclassical transport in the low-collisionality  $1/\nu$  regime is optimized using the NEO code<sup>14</sup> to evaluate a function  $\chi_{NEO}$  targeting values of the effective ripple factor  $\epsilon_{eff}^{3/2}$  on several magnetic flux surfaces. Subroutines interface each physics and engineering model with the optimization code, and several models [e.g., NEO, COBRA (Ref. 15), NESCOIL (Ref. 4), and TERPSICHORE (Ref. 16)] are executed

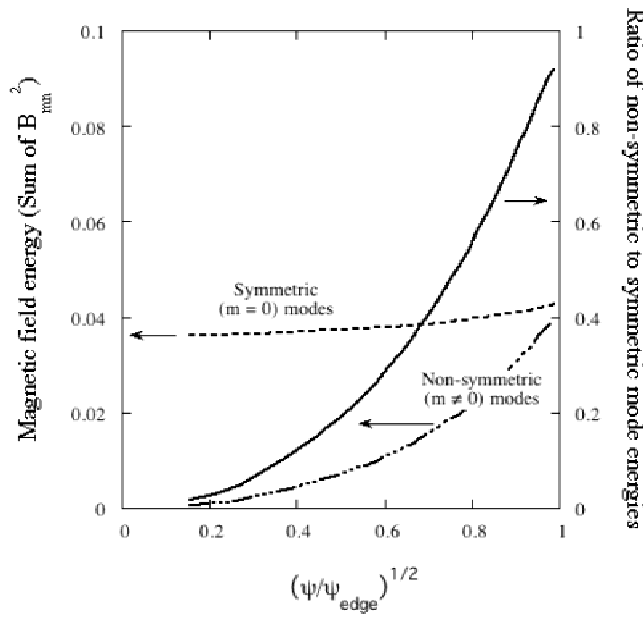


Fig. 2. The degree of quasi-poloidal symmetry versus the normalized radial coordinate (toroidal flux) in the QPS configuration, as measured by the ratio of energy in the nonsymmetric Fourier components of  $|\mathbf{B}|$  to the energy in the symmetric components.

through system calls from these subroutines. Data from these models are passed to the optimization code through files, therefore requiring minimal modification to the software provided by the model developer. This is computationally efficient because the time required for evaluation of the physics model is typically long compared to the file-based data transfer time. Parallelization<sup>17</sup> on high-performance computers is straightforwardly implemented at the level of the optimization algorithm (e.g., computing the gradient of  $\chi^2$ ) and *not* within individual physics and engineering modules.

The COILOPT code<sup>8</sup> is based on a parametric representation of coils confined to a coil winding surface (see Fig. 3)  $R = \sum_i R_i \cos[2\pi(m_i u + n_i v)]$ ,  $Z = \sum_i Z_i \sin[2\pi(m_i u + n_i v)]$ , and  $\varphi = 2\pi v/N_p$ , where  $u$  and  $v$  are the normalized poloidal and toroidal angles, respectively. The winding law for modular coils on this surface (see Fig. 4) is described as a function of  $u$  and  $v$  by either Fourier series or a cubic spline representation  $u(s) = \sum_j u_j B_j(s)$  and  $v(s) = \sum_j v_j B_j(s)$ . In the spline representation, the basis functions  $B_j(s) = B_j(s; t_j, \dots, t_{j+4})$  are normalized cubic B-splines<sup>18</sup> defined on the interval  $[0, 1]$  with a prescribed set of  $N + 4$  monotonically increasing knots  $t_j \in [0, 1]$ . The  $N$  pairs of coefficients  $(u_j, v_j)$  are referred to as “control points” (Fig. 4) and are constrained to satisfy periodic end conditions. Compared to the Fourier representation, splines allow control of *local* changes in coil geometry. Both the winding law coefficients and the coil currents are possible independent vari-

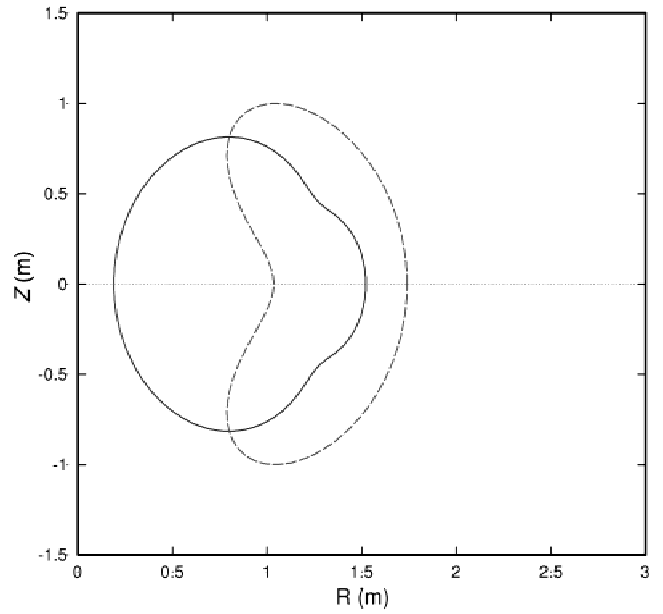


Fig. 3. The coil winding surface shown in the  $v = 0$  (dashed) and  $v = \frac{1}{2}$  (solid) toroidal symmetry planes.

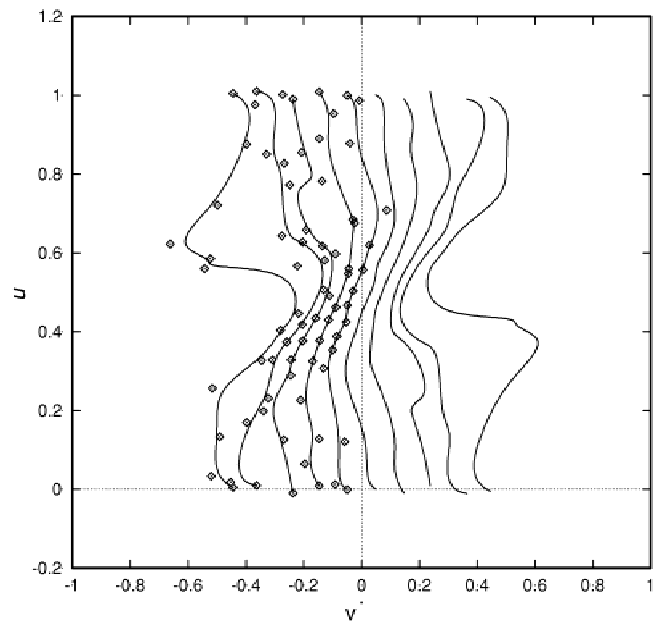


Fig. 4. Filaments for 10 (of 20) QPS winding packs, depicting the modular coil winding law. The control points of the cubic B-splines are shown for the five unique winding pack types.

ables for coil optimization. The components of the objective function in COILOPT include penalty functions presenting the normal component of the magnetic field on the targeted plasma surface as well as engineering constraints on the coil geometry.

In the merged plasma-coil optimization code, the state vector  $\mathbf{x}$  now consists of the independent variables from COILOPT (as described above), together with internal plasma profile coefficients from STELLOPT. In this merged model, COILOPT is executed in a “single-step” mode from a system call within STELLOPT to evaluate the coil engineering contributions to  $\chi^2$ . A solution is achieved by targeting *both* the physics parameters of the reference plasma *and* the geometric properties necessary for engineering coil design, while allowing the plasma boundary shape to vary in accordance with a free-boundary MHD equilibrium response to the external coils and currents.

### III. IMPLEMENTATION OF THE ROBUSTNESS (VACUUM FIELD) CONSTRAINT

Plasma flexibility and robustness are important components of stellarator coil design.<sup>19</sup> Of particular interest is the ability of a coil set to produce plasma configurations having a large fraction of nearly integrable surfaces over a wide range of beta values. Because the plasma properties and surface quality are optimized at full beta, there is no guarantee that the magnetic surface quality will be maintained at lower beta. Indeed, the vacuum magnetic flux surfaces are typically evaluated by integration of the field line equations

$$dR/d\varphi = RB_R/B_\varphi$$

and

$$dZ/d\varphi = RB_Z/B_\varphi \quad (1)$$

only *after* a coil configuration has been established by optimization at high beta. Here,  $(R, \varphi, Z)$  are cylindrical coordinates, and  $(B_R, B_\varphi, B_Z)$  are the respective cylindrical components of the magnetic field  $\mathbf{B}$ .

Heretofore, it has been difficult to directly influence this important vacuum equilibrium feature during the optimization process. In this work, a vacuum field term  $\chi_B = w_B |\mathbf{B} \cdot \mathbf{n}| / |\mathbf{B}|$  is added to the STELLOPT objective function  $\chi^2$  in an attempt to maintain flux surface integrity and robustness at low beta. Here,  $\mathbf{n}$  is the normal to the full-pressure plasma boundary,  $\mathbf{B}$  is the vacuum magnetic field due to the coils, and  $w_B$  is the weight assigned to this target. During optimization, this term is minimized to force the last closed vacuum magnetic flux surface to enclose the same volume as the full-pressure plasma. Evaluation of this function requires knowledge of the plasma boundary. Thus, COILOPT is called twice for each evaluation of  $\chi^2$ . The first call evaluates the coils needed to compute the free-boundary VMEC equilibrium. The next call then uses the computed plasma boundary to evaluate plasma-dependent constraints, including  $\chi_B$  and the minimum plasma-coil distance.

Numerical experience shows that to obtain a plasma volume bounded by good vacuum flux surfaces that is comparable to that for the high-beta equilibrium requires an average error  $\langle \delta B \rangle = (1/A) \int_{\partial P} |\mathbf{B} \cdot d\mathbf{A}| / |\mathbf{B}| \leq 1.3\%$  for the normal component of the vacuum magnetic field at the full-pressure plasma boundary  $\partial P$ .

### IV. DESIGN OPTIMIZATION FOR QPS

The QPS is a concept exploration experiment designed to investigate the effects of 3-D shaping and quasi-poloidal symmetry  $\partial |\mathbf{B}| / \partial \theta \approx 0$  ( $\theta$  is the poloidal angle in Boozer coordinates<sup>20</sup>) on neoclassical confinement at moderate beta in a very low aspect ratio compact stellarator ( $A \leq 2.7$ ). The QPS plasma has two field periods, average major radius  $\langle R \rangle = 0.95$  m, volume-averaged magnetic field  $\langle B \rangle = 1$  T, and infinite- $n$  ballooning stable limit  $\langle \beta \rangle = 2\%$ . The optimization targets used here are relevant to this near-term experiment (they would be necessarily different for a higher-beta or reactor design).

For the configuration considered here, the pressure profile was chosen to be parabolic in the normalized toroidal flux:  $p(s) = p_0(1 - s)^2$ . This profile and the computed flux-averaged toroidal current density  $\langle j \cdot \nabla \varphi \rangle$  are plotted in Figs. 5a and 5b versus the normalized toroidal flux  $s = \psi / \psi_{edge}$ . The current profile is determined as part of the optimization to be consistent with the low-collisionality value of the bootstrap current calculated for this  $|\mathbf{B}|$  spectrum.

The present nonplanar (modular) coil set in the QPS consists of 20 modular coils (described below), 12 TF coils capable of changing the toroidal field on axis by  $\pm 0.2$  T, and 3 pairs of circular VF coils. An additional engineering requirement for the QPS modular coils is a minimum space of 40 cm between the centerlines of coil winding packs across the center of the device for the TF legs and solenoid coils.

#### IV.A. Coil Engineering Properties

The winding packs each contain multiple turns of multistrand flexible copper conductor wound on a machined stainless steel winding form. In the present optimization, each winding pack was modeled with a single central filament. (Multifilament, finite-build coils have been shown to have minimal effects on the physics properties of the QPS configurations.) Originally, the QPS modular coil set had 32 winding packs, arranged in 16 coils consisting of 2 winding packs closely separated and supported by a thin “T”-shaped structural element. Because of stellarator symmetry, there were only four different types of coils. An early innovation in the QPS design was to allow one of the four coil types (the coils nearest the center of the field period, or the  $\nu = \frac{1}{2}$  symmetry plane) to have winding packs that follow independent (not parallel) paths (Fig. 6). This design featured a

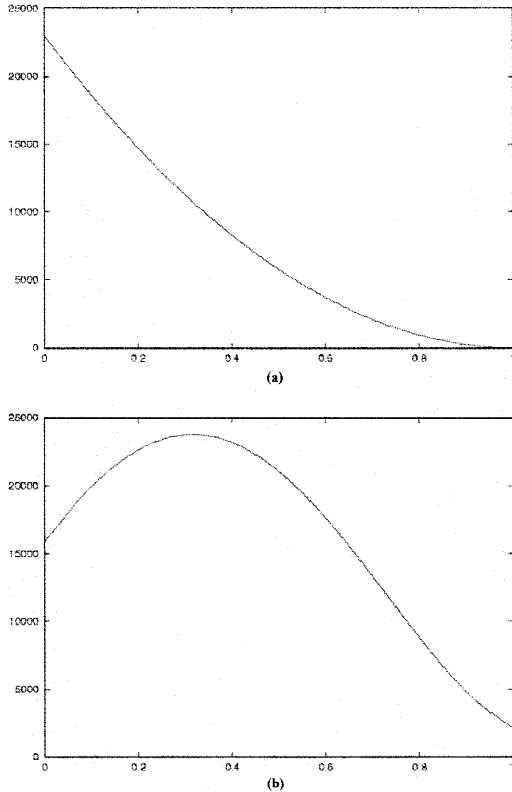


Fig. 5. (a) Pressure and (b) toroidal current profiles versus normalized toroidal flux  $s$  for the present QPS configuration.

structural web that connected (mechanically, but not electrically) the two winding packs of the split coil and varied in width along the trajectory of the coil. This provided the ability to create a more highly shaped magnetic field in the critical inboard region of the plasma near  $v = \frac{1}{2}$  without increasing either the total number of modular coils or the number of coil winding forms. The number of distinct winding form shapes, in particular, is a major cost driver in compact stellarator coil design.

A recent change in the QPS coil design was to allow *all* pairs of winding packs to have this variable web structure and to combine the winding packs *across* the  $v = \frac{1}{2}$  symmetry plane into a single stainless steel winding form. There are now two pairs of winding packs near the  $v = 0$  symmetry plane, which are wound on two spatially separated forms of the same type. Each coil now consists of a single  $7.1 \times 14.2$ -cm winding pack. This allows space near the  $v = 0$  plane for diagnostic access to the plasma and reduces the number of distinct winding forms from 4 to 3 (Fig. 7). The total number of coil winding forms is decreased from 16 to 10. There are now five different coil types. These changes significantly reduce the cost of the modular coils, compared to the earlier design.<sup>2</sup>

The new configuration was designed by adding individual coil-to-coil spacing constraints in COILOPT.

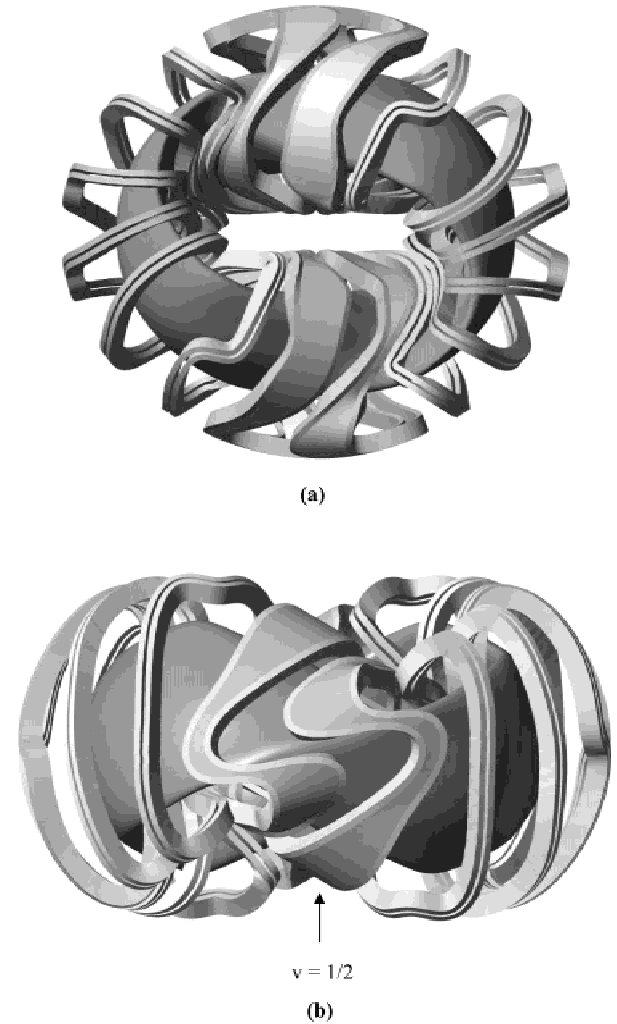


Fig. 6. (a) Top and (b) side views of modular coils for the original QPS configuration.<sup>2</sup> Pairs of winding packs were joined by a structural web to form separate coils. All pairs of winding packs were closely spaced except those near the  $v = \frac{1}{2}$  symmetry plane.

Previously, only a minimum distance  $\Delta_n^{(min)}$  to all other coils was targeted for each of the different coil types. The new optimization targets a matrix of minimum coil separation constraints, comparing each unique coil type  $n$  with a different coil  $m \neq n$ , i.e.,  $\chi_{n,m} = \max\{0, w_{n,m}(\Delta_{n,m}^{(target)} - \Delta_{n,m}^{(min)})\}$ . Here,  $w_{n,m}$  is the weight for this target. Thus, coils that are wound on the same winding form can be assigned a smaller separation target distance than those that are not joined by a structural web. This allows more spacing between coils in adjacent winding forms and the ability to orient the individual winding packs for improved fabricability.

Table I compares the reconfigured coil system obtained using the vacuum field constraint (designated case 022103a), with the earlier QPS design.<sup>2</sup> Filamentary coils

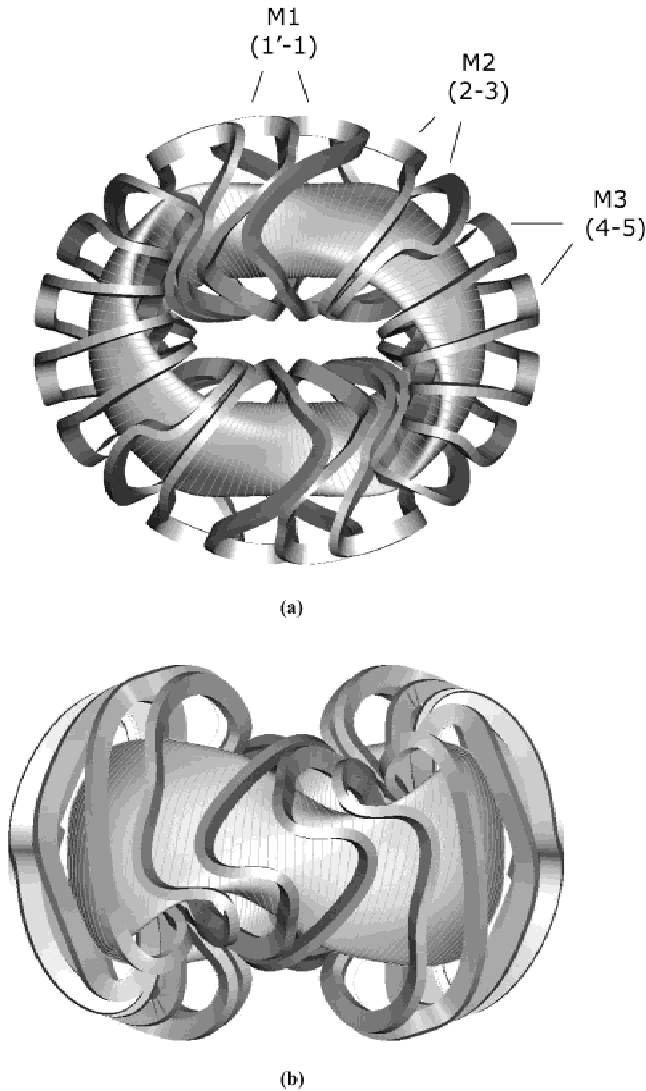


Fig. 7. (a) Top and (b) side views of modular coils for the present (improved) QPS configuration. Coil pairs 1' and 1, 2 and 3, and 4 and 5 are wound on the same winding form and are connected by a structural web (not shown) that varies in width along the coil trajectories.

were used in the comparison. While both configurations have comparable aspect ratios ( $\sim 2.65$  to  $2.75$ ), other plasma properties have improved in the reconfigured design. Plasma volume and ballooning-stable beta both increased. Neoclassical confinement in the  $1/\nu$  regime, characterized here by the effective ripple at  $r/a \sim 0.7$  (corresponding to the normalized toroidal flux  $s = 0.5$ ), also improved, as indicated by a decrease in the ripple transport by a factor of  $\sim 2.6$ . This is directly correlated in the QPS with a reduction of neoclassical poloidal viscosity, so the present design should allow greater control of the poloidal rotation needed for reduction of anomalous transport.

TABLE I

Comparison of an Improved QPS Plasma and Coil Optimization (Case 022103a) with the Original Configuration<sup>2\*</sup>

Optimization Target	Original QPS	Case 022103a
A, aspect ratio	2.65	2.76
Volume (m <sup>3</sup> )	1.81	2.27
Bootstrap current (kA)	45.9	37.8
Ballooning beta— <i>n</i> infinite (%)	1.83	2.00
Ripple diffusion $\times 10^3$ ( $s = 0.5$ )	3.53	1.35
Iota at maximum beta		
$s = 0$	0.293	0.281
$s = 0.5$	0.341	0.324
$s = 1.0$	0.345	0.329
Normal vacuum field error (% , $s = 1$ )		
Average	1.82	1.27
Maximum	6.45	4.34
Minimum coil-plasma separation (cm)	13.0	15.4
Minimum coil separation (cm)		
Winding pack 1'-1	14.9	9.4
Winding pack 1-2	6.1	13.0
Winding pack 2-3	9.6	10.4
Winding pack 3-4	11.0	13.1
Winding pack 4-5	13.8	13.9
Winding pack 5-5'	18.0	18.1
Minimum radius of curvature (cm)		
Winding pack 1	9.3	12.8
Winding pack 2	9.4	12.3
Winding pack 3	11.0	12.2
Winding pack 4	12.4	15.3
Winding pack 5	14.2	16.4
Total coil length (m)	90.4	101.6
Maximum coil R (m)	1.64	1.73
Minimum distance across center, Y (cm)		
Winding pack 1	36.0	40.0
Winding pack 2	37.0	43.4
Winding pack 3	38.2	40.0

\*Distances are to the center of the winding packs, and ripple diffusion is in arbitrary units.

The coil engineering features of the new configuration are significantly improved (Table I) compared with the original QPS design.<sup>2</sup> The minimum separation between the confined plasma and the coil centerline (plasma-coil separation), which is a measure of the plasma scrape-off needed for adequate divertor operation, has increased by  $>2$  cm ( $\sim 18\%$ ). The minimum coil-coil separation is also larger, which allows the size and shape of the winding packs to be optimized for maximum conductor area. Preliminary layouts show that increased conductor area reduces the current density by  $\sim 20\%$ , which will in turn provide greater experimental flexibility. The implied radial build indicates a scrape-off distance of  $\sim 8$  cm.

In addition to improved coil-to-coil separations, the new configuration also has a more uniform arrangement

of “paired” and “unpaired” coils. This allows the twist of the coil cross section to more closely match a free-form or developable orientation.<sup>21</sup> The geometry of the supporting structure is also improved, with more space between coils in the region of the assembly joint of the two field periods. In the new configuration, the minimum distance across the center of the torus is larger by 4 cm. This space is used to accommodate the inner leg of the TF coils, the Ohmic solenoid, and the vacuum casing. The additional space can be used to optimize the central structure and flux capability of the solenoid.

Other important parameters that have been considered in the optimization process are radius of curvature, or bend radius, of the winding center; total coil length; and overall dimensions of the coil set. In the new configuration, small increases in coil length and maximum major radius are offset by an increase in the minimum bend radius from 9.3 to >12.2 cm. Bend tests with a prototypical conductor indicate that this change greatly improves the feasibility of winding coils without excessive distortion of the winding.

**IV.B. Magnetic Surface Quality**

Vacuum magnetic surfaces for the new configuration are compared with those of previous designs in Figs. 8, 9, and 10, which show the surfaces in the  $\nu = \frac{1}{2}$  symmetry plane. The original QPS design<sup>2</sup> was chosen for its low aspect ratio in both vacuum (Fig. 8) and at finite beta, as well as good transport and stability characteristics. Optimization of this configuration to improve its coil engineering properties *without* applying

the vacuum constraint produced a plasma with a substantially smaller volume of nested magnetic surfaces (Fig. 9).

In the new configuration (Fig. 10), the vacuum normal field error has been significantly reduced at the

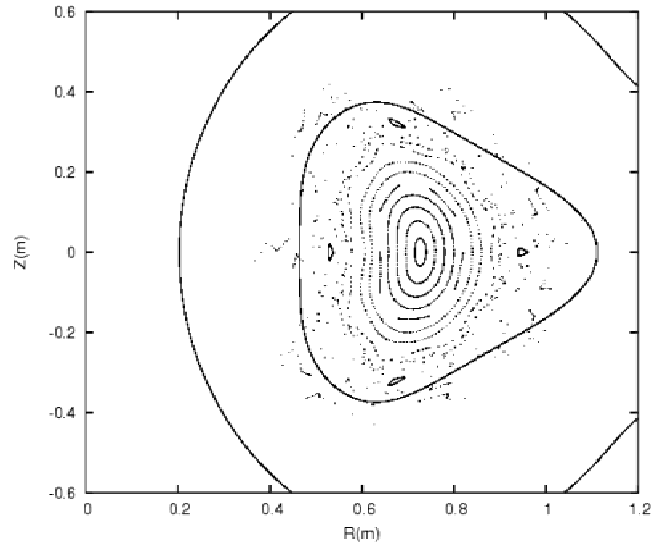


Fig. 9. Vacuum magnetic surfaces in the  $\nu = \frac{1}{2}$  symmetry plane for the reconfigured coils with improved physics properties *before* application of the vacuum constraint. The outer solid line is the coil winding surface, and the inner solid line is the full-beta VMEC plasma boundary.

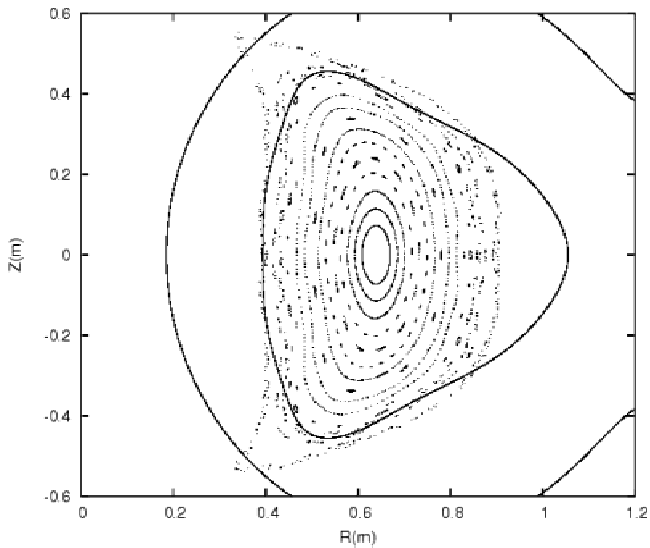


Fig. 8. Vacuum magnetic surfaces in the  $\nu = \frac{1}{2}$  symmetry plane for the original QPS configuration.<sup>2</sup> The outer solid line is the coil winding surface, and the inner solid line is the full-beta VMEC plasma boundary.

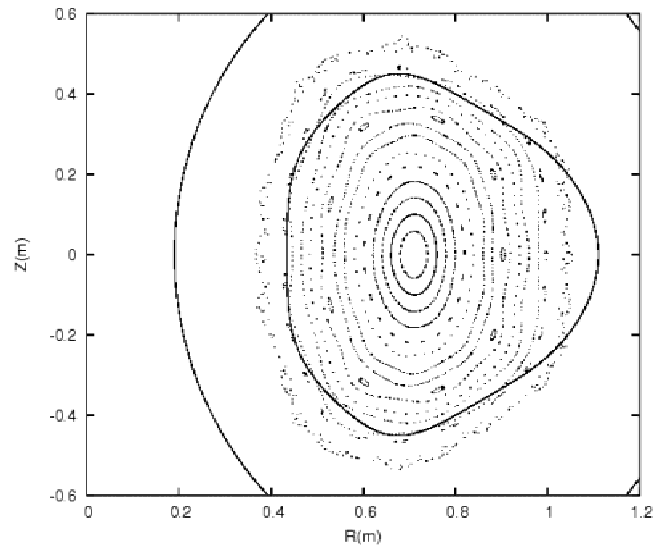


Fig. 10. Vacuum magnetic surfaces in the  $\nu = \frac{1}{2}$  symmetry plane for the improved coil (and physics) configuration (case 022103a), *after* applying the vacuum constraint. The outer solid line is the coil winding surface, and the inner solid line is the full-beta VMEC plasma boundary.

location of the full-beta boundary (see Table I). (The coil currents are the same as those for the full-beta case and were not further optimized for low beta.) This yielded a plasma volume and aspect ratio in vacuum that were comparable to that of the full-beta case. Also, a large fraction of the volume consisted of closed magnetic surfaces (compared to islands). The preservation of aspect ratio with beta is important because QPS experiments that focus on neoclassical transport reduction will be conducted at low beta.

A small ( $n = 2, m = 9$ ) island chain is seen in Fig. 10. Island chains such as this may be targeted through the variation of coil currents (within the bounds set by power supply capability) and, if necessary, the addition of small correction coils. Both this and the ( $n = 2, m = 8$ ) resonance that are present in the vacuum iota profile (Fig. 11) migrate toward the magnetic axis and disappear with increasing beta and bootstrap current. At the maximum ballooning-stable value of  $\beta \sim 2\%$ , about one-fourth of the total transform at the plasma edge is produced by the self-consistent bootstrap current of  $\sim 38$  kA. Thus, magnetic islands do not seem to be an issue at higher beta. A recent PIES calculation<sup>22</sup> shows only a small ( $n = 6, m = 19$ ) island chain in the plasma and an outer flux surface that is larger than the original VMEC surface. In addition, the equilibrium bootstrap current is lower in the new configuration despite the higher beta and larger plasma volume, so there is a smaller difference between the iota profiles at low and full beta, as shown in Fig. 11.

#### IV.C. Transport Properties

The achievement of low levels of neoclassical transport has been one of the important targets in our physics optimization. To verify that the new configuration described in Table I meets this goal, we have evaluated its

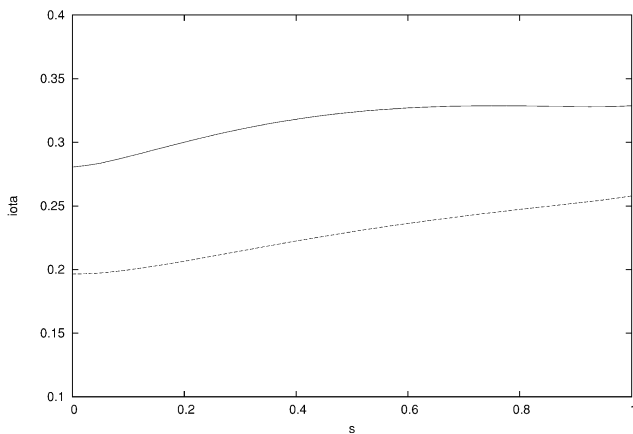


Fig. 11. Iota profiles for the present QPS coil configuration versus the normalized toroidal flux  $s$  for vacuum (dashed) and  $\langle\beta\rangle = 2\%$  (solid). The difference is due to the self-consistent bootstrap current.

transport properties using several different tools and compared the results with the earlier QPS design.

One of the significant ways in which stellarator transport differs from that in axisymmetric tokamaks is in the low-collisionality regime where neoclassical transport coefficients in the stellarator scale as  $1/\nu$  (until nonlocal superbanana effects become dominant at very low collisionality). In contrast, tokamak transport coefficients continue to decrease as  $\nu$  at low collisionalities. The overall level of the  $1/\nu$  transport is determined by the effective ripple  $\epsilon_{eff}^{3/2}$ . In designing low-aspect-ratio configurations, it has thus been important to minimize this effective ripple. The NEO code<sup>14</sup> has provided a rapid and accurate means for evaluating the level of ripple for an arbitrary spectrum of the magnetic field strength  $|\mathbf{B}|$ . A plot of the effective ripple coefficients for case 022103a and the earlier QPS designs is shown in Fig. 12. There is a significantly lower ripple level over most of the plasma cross section in the present configuration.

An alternative way of evaluating transport in non-axisymmetric systems is to use Monte Carlo calculations that follow a large number of particle orbits in time and record the loss rates as the particles exit the plasma volume. The global particle and energy lifetimes can then be estimated by recording the energy lost as particles

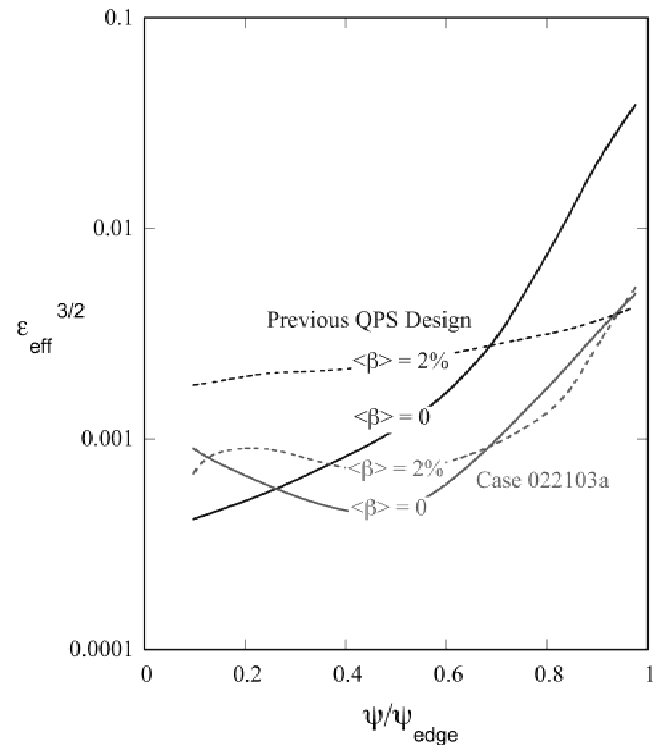


Fig. 12. Effective ripple coefficient  $\epsilon_{eff}^{3/2}$  calculated from the NEO code<sup>14</sup> versus normalized flux (radial position) for the present case 022103a and the previous QPS case.<sup>2</sup>

leave the confined volume and then reseeding them back into the plasma according to a probability distribution function that models prescribed temperature and density profiles. Such a calculation runs until the losses reach a quasi steady state. In Figs. 13a and 13b, such a model was applied to compute the thermal ion confinement in the two QPS devices described in Table I. In Fig. 13a, plasma parameters that characterize an ion cyclotron radio frequency (ICRF)-heated regime are used:  $n(0) = 8.3 \times 10^{19} \text{ m}^{-3}$ ,  $T_{ion}(0) = 500 \text{ eV}$ , and  $T_{electron}(0) = 500 \text{ eV}$ .

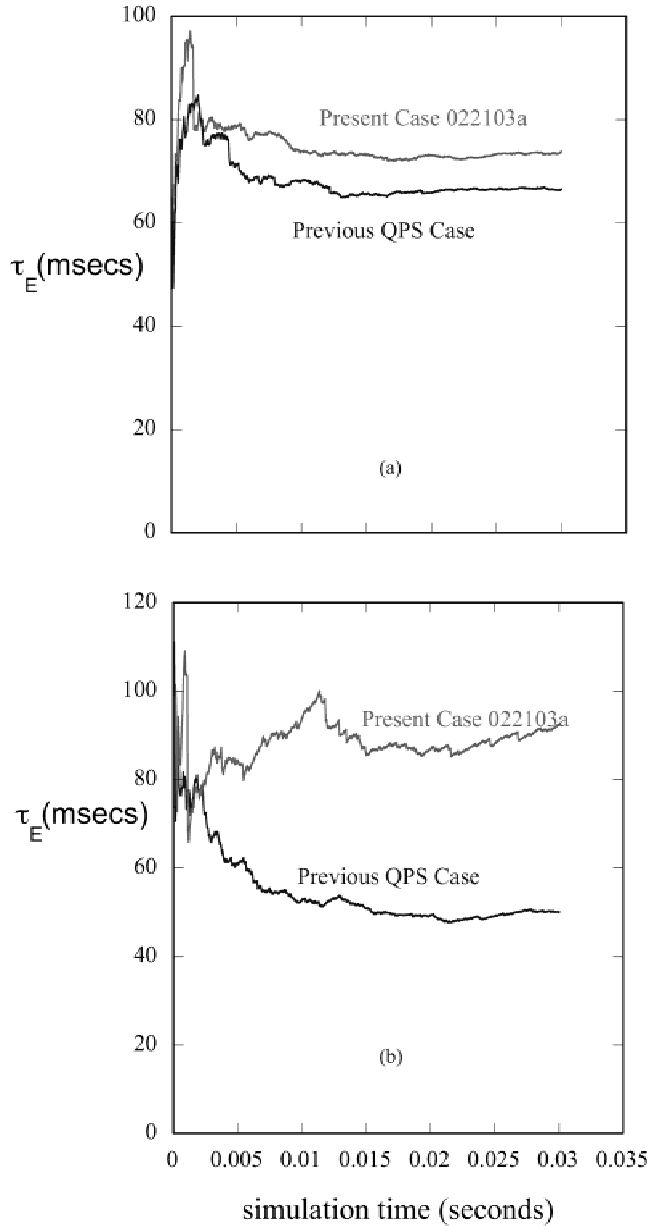


Fig. 13. Monte Carlo thermal ion energy lifetimes for the present configuration and the previous QPS case<sup>2</sup> based on (a) ICRF regime parameters and (b) ECRF parameters.

In Fig. 13b, plasma parameters that characterize a lower-density electron cyclotron radio frequency (ECRF)-heated regime are used:  $n(0) = 1.8 \times 10^{19} \text{ m}^{-3}$ ,  $T_{ion}(0) = 150 \text{ eV}$ , and  $T_{electron}(0) = 1400 \text{ eV}$ . In both regimes, the present configuration offers higher-energy confinement times than the earlier QPS device.

A unique physics feature of the QPS device arising from its quasi-poloidal symmetry is a much lower level of viscous flow damping in the poloidal direction as compared to the flow damping in the toroidal direction. This viscous anisotropy is reversed compared to that in a tokamak, which is characterized by a toroidal viscosity that is much lower than the poloidal viscosity. As a result of the connection between the poloidal viscosity and the generation of the sheared flows that are thought to be necessary for enhanced confinement regimes, QPS configurations may offer improved access to such regimes. Recently, a theoretical framework has been developed<sup>23</sup> that allows the calculation of the viscosity tensor coefficients for nonaxisymmetric systems using the DKES neoclassical transport model.<sup>24</sup> We have applied this formulation to the QPS configurations discussed above to compute the normalized viscosity coefficient profiles shown in Fig. 14. These coefficients relate the flux-surface-averaged poloidal and toroidal components of

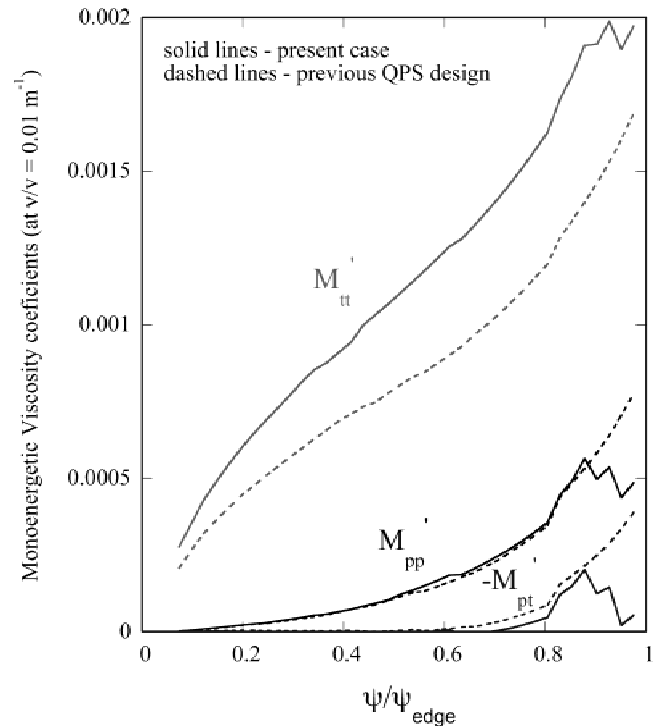


Fig. 14. The components of the viscosity tensor  $M'_{tt}, M'_{pt}, M'_{pp}$  for a fixed energy corresponding to  $\nu/v = 0.01 \text{ m}^{-1}$  versus flux surface position for the present QPS configuration 0221023a (solid lines) and the previous QPS case<sup>2</sup> (dashed).

the viscous stresses to the in-surface, averaged components of the flow velocity through the following equations:

$$\begin{pmatrix} \langle \mathbf{B}_p \cdot \nabla \cdot \boldsymbol{\pi} \rangle \\ \langle \mathbf{B}_t \cdot \nabla \cdot \boldsymbol{\pi} \rangle \end{pmatrix} = \begin{bmatrix} M_{pp} & M_{pt} \\ M_{tp} & M_{tt} \end{bmatrix} \begin{pmatrix} \langle u^p \rangle \\ \langle u^t \rangle \end{pmatrix}. \quad (2)$$

For  $i$  (and  $j$ )  $\in (p, t)$ ,  $M_{ij}$  are the coefficients  $M_{a1ij}$  given in Eq. (39) of Ref. 23 (with  $a = \text{ion}$ ) in terms of the normalized viscosity coefficients  $M'_{ij} \equiv M_{a1ij}(K)/4\pi^2 m_a v_{Ta} K^{3/2}$ , where  $K = E/T_a$  is the normalized particle energy. Here,  $u^p = \mathbf{u} \cdot \nabla \theta / \chi'$  and  $u^t = \mathbf{u} \cdot \nabla / \psi'$  are the normalized poloidal and toroidal flows, respectively.

For both configurations, the poloidal viscosity coefficient ( $M'_{pp}$ ) is substantially less than the toroidal viscosity coefficient ( $M'_{tt}$ ). This is a direct consequence of attempting to impose quasi-poloidal symmetry on the spectrum of  $|\mathbf{B}|$  during the optimization. The present configuration (022103a) has a higher ratio between the toroidal and poloidal viscosities than the earlier QPS configuration<sup>2</sup> (this ratio approaches  $\infty$  for a perfectly quasi-poloidal symmetry design).

#### IV.D. Stability Properties

The optimization included stability targets for both Mercier (interchange) and infinite- $n$  ballooning at  $\langle \beta \rangle \sim 2\%$ . These were computed numerically using the COBRA code.<sup>15</sup> Stability to finite- $n$  ballooning modes, as well as kink and vertical modes, was evaluated (as a postprocessing calculation) using the TERPSICHORE code.<sup>16</sup>

Stability calculations were performed using the quadratic pressure profile shown in Fig. 5a. For this pressure profile (which is *not* optimized for stability), the previous QPS plasma<sup>2</sup> became unstable to infinite- $n$  ballooning modes at  $\langle \beta \rangle = 2.1\%$  and the present case at a slightly lower pressure,  $\langle \beta \rangle = 1.9\%$ . For finite- $n$  ballooning modes (up to  $n = 19$ ), the beta limits were somewhat higher,  $\langle \beta \rangle \sim 2.5\%$ , in both configurations.

Ballooning beta limits can be increased by optimizing the pressure profile. For both configurations, the infinite- $n$  ballooning mode stability limit can be raised by using such profiles to  $\langle \beta \rangle \sim 2.4\%$ , which is somewhat higher than the expected maximum pressure for the QPS experiment.

Kink and vertical modes become unstable for these types of QPS plasmas for even larger pressures:  $\langle \beta \rangle \sim 4\%$ .

#### V. SUMMARY

The capability for numerical optimization of compact stellarator plasmas and coils has been extended by adding a vacuum field constraint to the merged STELLOPT/COILOPT design code. This new target attempts to minimize the normal component of the *vacuum*

magnetic field at the *full-pressure* plasma boundary. The resulting plasma has a last-closed vacuum magnetic flux surface that encloses a plasma volume comparable to, or exceeding, that at the highest beta values, thus maintaining the plasma aspect ratio as beta is varied. The configuration shows some of the invariance to beta variations exhibited by the W7-X design,<sup>6</sup> while sustaining a nonzero bootstrap current for  $\beta > 0$ . The application of this vacuum field constraint, together with a reconfiguration of the modular coils, has led to the improved physics performance and engineering flexibility, as well as lower project cost, of the present QPS design.

#### ACKNOWLEDGMENTS

The research was sponsored by Oak Ridge National Laboratory, managed by UT-Battelle, LLC, for the U.S. Department of Energy under contract DE-AC05-00OR22725. We thank J. A. Rome for carefully reading the manuscript and providing helpful comments.

#### REFERENCES

1. G. H. NEILSON et al., "Physics Issues in the Design of High-Beta, Low-Aspect-Ratio Stellarator Experiments," *Phys. Plasmas*, **7**, 1911 (2000).
2. J. F. LYON et al., "Physics Issues for a Very-Low-Aspect-Ratio Quasi-Poloidal Stellarator (QPS)," *Proc. 19th Fusion Energy Conf.*, Lyon, France, October 2002, International Atomic Energy Agency (2002); see also B. E. NELSON et al., "Engineering Aspects of Compact Stellarators," *Proc. 19th Fusion Energy Conf.*, Lyon, France, October 2002, International Atomic Energy Agency (2002).
3. J. NÜHRENBERG and R. ZILLE, *Phys. Lett. A*, **114**, 129 (1986).
4. P. MERKEL, *Nucl. Fusion*, **27**, 5, 867 (1987).
5. M. DREVLAK, "Automated Optimization of Stellarator Coils," *Fusion Technol.*, **33**, 106 (1998).
6. G. GRIEGER et al., *Proc. 13th Int. Conf. Plasma Physics and Nuclear Fusion Research*, Washington, D.C., October 1–6, 1990, Vol. 3, p. 525, International Atomic Energy Agency (1991).
7. D. A. SPONG et al., *Nucl. Fusion*, **41**, 711 (2001).
8. D. J. STRICKLER, L. A. BERRY, and S. P. HIRSHMAN, "Designing Coils for Compact Stellarators," *Fusion Sci. Technol.*, **41**, 107 (2002).
9. J. J. MORÉ, B. S. GARBOW, and K. E. HILLSTROM, "Users Guide to MINPAC-I," Argonne National Laboratory (1980).
10. D. J. STRICKLER et al., "Integrated Plasma and Coil Optimization for Compact Stellarators," *Proc. 19th Fusion*

- Energy Conf.*, Lyon, France, October 2002, International Atomic Energy Agency (2002).
11. S. P. HIRSHMAN and J. C. WHITSON, *Phys. Fluids*, **26**, 3553 (1983).
  12. J. R. CARY and J. D. HANSON, *Phys. Fluids*, **29**, 2464 (1986).
  13. S. R. HUDSON et al., *Phys. Rev. Lett.*, **89**, 275003 (2002).
  14. V. V. NEMOV et al., *Phys. Plasmas*, **6**, 4622 (1999).
  15. R. SANCHEZ et al., *J. Comput. Phys.*, **161**, 576 (2000).
  16. D. V. ANDERSON et al., *J. Supercomput. Appl.*, **4**, 34 (1990).
  17. D. A. SPONG et al., "QPS Plasma and Coil Optimization," presented at 13th Int. Stellarator Workshop, Canberra, Australia, February 2002.
  18. C. DE BOOR, *A Practical Guide to Splines*, Springer-Verlag, New York (1978).
  19. N. POMPHREY et al., "Flexibility and Robustness Calculations for NCSX," PPPL-3701, Princeton Plasma Physics Laboratory (June 2002).
  20. A. H. BOOZER, "Plasma Equilibrium with Rational Magnetic Surfaces," *Phys. Fluids*, **24**, 1999 (1981).
  21. P. L. WALSTROM, "Twisted Coil Geometry in Plasma Confinement Devices," *J. Fusion Energy*, **3**, 265 (1987).
  22. D. MONTICELLO, Personal Communication (2003).
  23. H. SUGAMA and S. NISHIMURA, "How to Calculate the Neoclassical Viscosity, Diffusion, and Current Coefficients in General Toroidal Plasmas," *Phys. Plasmas*, **9**, 4637 (2002).
  24. W. I. VAN RIJ and S. P. HIRSHMAN, "Variational Bounds for Transport Coefficients in Three-Dimensional Toroidal Plasmas," *Phys. Fluids B*, **1**, 563 (1989).

---

**Dennis J. Strickler** (BA, mathematics, Berea College, 1971; MA, mathematics, University of Kentucky, 1973) is a research staff member in the Computational Sciences and Engineering Division at Oak Ridge National Laboratory (ORNL). His current responsibilities and research interests are in the area of magnetic coil design for compact stellarators.

**Steven P. Hirshman** [EE, MS, 1973, and ScD, 1976, electrical engineering, Massachusetts Institute of Technology (MIT)] is a senior research staff scientist in the Fusion Energy Division at ORNL. His research interests include theoretical modeling and simulation of equilibrium and transport in three-dimensional (3-D) toroidal plasma configurations.

**Donald A. Spong** (BS, 1970, nuclear engineering, University of Arizona; MSE, 1971, and PhD, 1976, nuclear engineering, University of Michigan) is a senior research staff member and stellarator theory group leader in the Fusion Energy Division at ORNL. His current research interests include stellarator neoclassical transport, stellarator optimization, particle simulation of energetic populations, Alfvén instabilities and magnetohydrodynamics in 3-D systems, and flux surface fragility in compact stellarators.

**Michael J. Cole** (BS, mechanical engineering, Memphis State University, 1973) is a research and development (R&D) staff member in the Fusion Energy Division at ORNL. His current responsibilities and research interests include the mechanical design and analysis of tokamak systems and compact stellarators.

**James F. Lyon** (BS, MS, and EE, electrical engineering, MIT, 1964; PhD, physics, University of Tennessee, 1970) is the stellarator program coordinator in the Fusion Energy Division at ORNL, where he serves as Quasi-Poloidal Stellarator (QPS) project head, National Compact Stellarator Experiment (NCSX) deputy project manager, and Large Helical Device (LHD) experimentalist. His current research interests are in stellarator physics and design, reactor systems optimization, fast ion measurements, and flux surface calculations.

**Bradley E. Nelson** (BS and MS, mechanical engineering, University of Missouri, 1976) is an R&D staff member in the Fusion Energy Division at ORNL. His current responsibilities and research interests are in the engineering design of compact stellarator experiments.

**David E. Williamson** (BS, mechanical engineering, University of Tennessee) is a research staff member in the Fusion Energy Division at ORNL. His current responsibilities and research interests are in the area of magnetic coil design for compact stellarators.

**Andrew S. Ware** (BS, physics, University of Texas, 1988; PhD, physics, University of California, San Diego, 1992) is an associate professor of physics at the University of Montana. His current research interests include the equilibrium and stability of stellarator plasmas, plasma turbulence and turbulent transport, and turbulence in geophysical fluids.